16th World Conference on Earthquake, 16WCEE 2017
Santiago Chile, January 9th to 13th 2017
Paper N° 3025
Registration Code: S-J1463158968

SENSITIVITY OF INDUCED SEISMICITY RISK TO SOURCE CHARACTERIZATION, GROUND MOTION PREDICTION, AND EXPOSURE

A. Gupta[1], J. W. Baker[2]

[1] PhD Candidate, Stanford University, abhineet@stanford.edu
[2] Associate Professor, Stanford University, bakerjw@stanford.edu

Abstract

We evaluate the impact of earthquake magnitude distribution, ground motion prediction equations, and exposure on repair cost risk for induced seismicity at a site in Oklahoma City in the United States. There has been a significant increase in earthquakes in some of the traditionally low seismicity regions of the Central and Eastern US. Here, we perform sensitivity analyses of various components that affect seismic risk to determine how the variability in measurements of these components affect the variability in estimated risk. For example, a 100-fold change in earthquake activity rate increases the hazard 100-fold; whereas alternative earthquake magnitude distributions, with maximum magnitudes of 6 versus 7, have little impact on risk. We assess the impacts of earthquake activity rate, magnitude distribution, and ground motion prediction equations on seismic hazard and repair cost risk, and the impact of exposure on risk. These sensitivity analyses can be used to identify those components that are more critical for risk assessment, and hence would benefit the most from better constraints. This information can be beneficial for better allocation and prioritization of the limited resources, and for data collection of the more critical factors that impact risk from induced seismicity.

Keywords: seismic hazard; seismic risk; sensitivity analysis

1. Introduction

In this paper, we analyze the sensitivity of seismic hazard and risk to magnitude distribution, and ground motion prediction equations in regions of induced seismicity. Seismicity generated as a result of human activities is referred to as induced or triggered seismicity. We analyze the sensitivity of repair cost risk to exposure. We also estimate this risk for a census block in Oklahoma City based on the induced seismicity hazard curves prepared by United States Geological Survey (USGS) [1], and the vulnerability and exposure data from HAZUS [2].

The motivation for this paper is the significant increase in seismicity that has been recently observed in the Central and Eastern US (CEUS) [3]. For example, in 2014 and 2015, more earthquakes of magnitude ≥ 3 were observed in Oklahoma than in California. There is a possibility that this increased seismicity is a result of underground wastewater injection [e.g., 3, 4, 5].

There is a need to understand and manage the increased hazard and risk from induced seismicity [6, 7]. The increased seismicity due to anthropogenic processes affects the safety of buildings and infrastructure, especially since seismic loading has historically not been the predominant design force in most CEUS regions. To assist this effort, USGS published one-year hazard maps for regions of induced seismicity [1]. In this paper, we develop the seismic risk using these updated hazard maps, and compare it with the risk from excluding the recent seismicity. We then analyze how various components in the USGS logic tree for hazard assessment affect both the hazard and risk. Researchers have previously estimated the hazard and risk from induced seismicity at an enhanced geothermal site in Basel, Switzerland [8]. Understanding the impact of different components can assist in deciding how to best allocate resources for risk estimation and mitigation.

In section 2, we calculate the risk for a census block in Oklahoma City using the USGS 2016 one-year hazard map. In section 3, we describe the parameter values for which sensitivity analyses are performed. In section 4, we present the results of the sensitivity analyses.

2. Estimating Risk in Oklahoma City

In this section, we estimate the repair cost risk for a census block in Oklahoma City (OKC), which has traditionally been a low-seismicity region. The building inventory data is obtained from HAZUS [2] for the census block at 35.5° N and 97.5° W, and is shown in Table 1. We calculate the risk in this block using the hazard curves prepared by USGS in their 2014 National Seismic Hazard Maps (NSHM) which excluded induced seismicity [9] (referred henceforth as 2014NatOnly), and their 2016 one-year maps which include induced seismicity [1] (referred henceforth as 2016Induced). These hazard curves are shown in Fig. 1. For comparison with a high-seismicity region, the hazard curve for Los Angeles (LA), California (34.04° N and 118.24° W, Site Class B/C) from 2014NatOnly is also shown.

Table 1 - Building type composition and fragility function medians for a census block in Oklahoma City, from HAZUS. Some building categories are compressed into *Others*.

Building classification	**Building % (by cost)**	**Building count**	**Building cost ($)**	**Damage state median PGA (g)**			
				Slight	*Moderate*	*Extensive*	*Complete*
W1 Wood, light frame	61.23%	89	28,487,479	0.20	0.34	0.61	0.95
W2 Wood, commercial and industrial	3.84%	6	1,784,800	0.14	0.23	0.48	0.75
UFB3 Unreinforced fire brick masonry	19.32%	9	8,990,071	0.14	0.20	0.32	0.46
Ot Others	10.97%	12	5,104,547	0.13	0.17	0.27	0.46
MH Mobile homes	4.64%	7	2,156,556	0.11	0.18	0.31	0.60

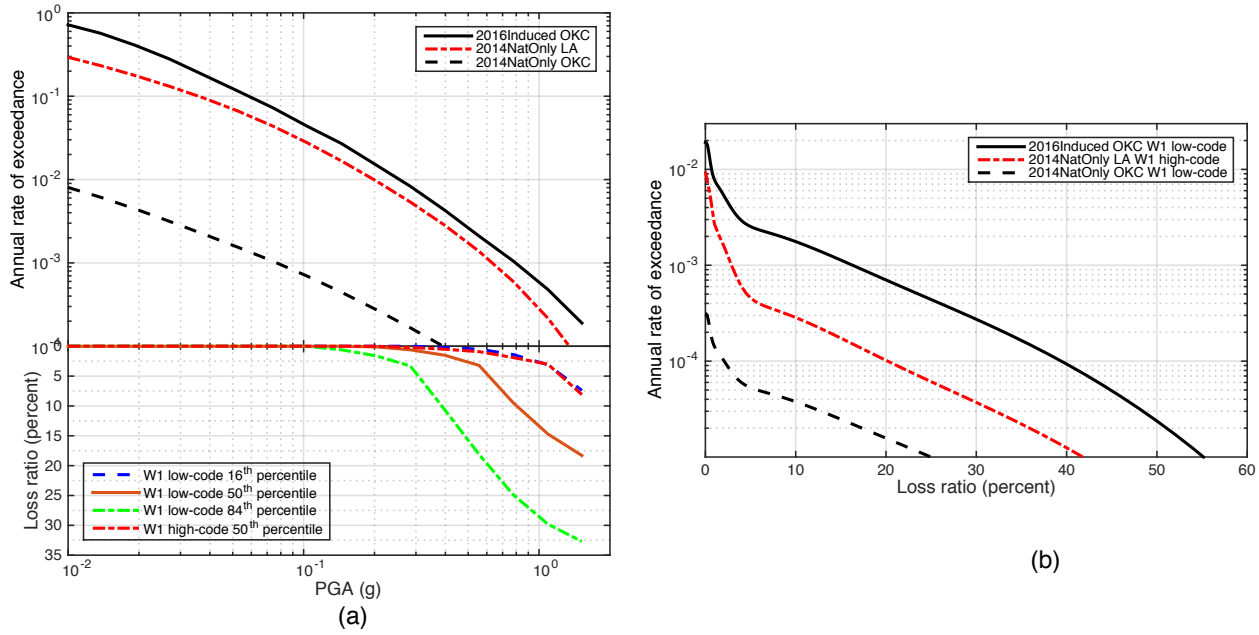

Figure 1 – (a) top: USGS hazard curves for Oklahoma City from 2014 NSHM, 2016 Induced Seismicity report, and for Los Angeles from 2014 NSHM. (a) bottom: Percentiles for loss ratios for W1 (light frame wood) at different PGA levels. (b): Risk curves for a single W1 structure, computed by combining hazard curves with probability of loss at a given PGA.

The seismic risk describes the rate of exceedance for a given loss value, in a similar manner as the seismic hazard describes the rate of exceedance for a given ground shaking level. The loss can be in terms of various components like repair cost, downtime cost, or number of people affected. Here, we compute the losses associated with only the structural components of buildings based on the fragility functions and loss values from HAZUS [2]. Henceforth in this paper, we use the term "risk" to refer to the risk associated with these structural losses.

A fragility curve describes the probability of exceeding a damage state for a given level of ground shaking, and it is specified by a lognormal cumulative distribution function in HAZUS [2]. We use the HAZUS fragility functions based on peak ground acceleration (PGA) as the measure of ground shaking. We assume low-code structural design at our site of interest since Oklahoma is in low-seismicity region. The definitions of low-code, moderate-code, and high-code terminology are given in HAZUS documentation [2]. Typically, regions with low expected seismicity like Oklahoma have low-code construction, and regions with high expected seismicity like California have high-code construction. The median PGA in units of **g** (gravity acceleration) for fragility functions corresponding to damage states - slight, moderate, extensive, and complete - are given in Table 1 for different building types. The log standard deviation for all building types and damage states is 0.64. We have compressed the original HAZUS table by combining the non-commercial building types with less than 5% cost, into the category - *Others*. The median PGA for this category is calculated as the average of the median PGA of the buildings comprising it.

To convert the damage state into loss values, HAZUS also provides the expected loss ratios for each damage state. The loss ratio defines the loss as a ratio of the total building cost. Some authors have suggested using a Beta distribution for damage-to-loss curves [10]. This distribution, or loss curve, gives the probability of loss at a given damage state. Here, we have assumed the losses to follow a Beta distribution with mean as given by HAZUS, and a coefficient of variation equal to 0.5. From HAZUS, we use the Mobile Home classification for MH, Industrial classification for W2, and Residential Single Family Dwelling for all other building types. The mean loss ratios for each damage state are given in Table 2.

Table 2: Damage to loss factors for building types in Oklahoma City, from HAZUS.

Occupancy classification	Loss ratio mean (%)				Applies to
	Slight	*Moderate*	*Extensive*	*Complete*	
RES1, Residential, single family dwelling	0.5	2.3	11.7	23.4	W1, UFB3, Ot
RES2, Residential, mobile home	0.4	2.4	7.3	24.4	MH
IND1, Industrial	0.4	1.6	7.8	15.7	W2

We can compute risk curves by combining the fragility functions, and the loss functions with the hazard curve at a site. The seismic risk describes the rate of exceedance of a given loss value, and a risk curve shows this rate over a range of loss values. The risk for loss value, x, for a single structure is computed using Eq. (1) [11].

$$\lambda(Loss > x) = \sum_{i=1}^{n_{DS}} P(Loss > x \mid ds_i) \sum_{j=1}^{n_{IM}} P(DS = ds_i \mid im_j)\lambda(IM = im_j) \quad (1)$$

where $\lambda(E)$ represents the rate of event E, $P(E)$ is the probability of event E, $P(E \mid A)$ is the probability of event E given event A, IM is an intensity measure, DS is a damage state, n_{DS} is the number of discrete damage states, and n_{IM} is the number of discrete intensity measures at which the hazard is calculated. $P(Loss > x \mid ds_i, im_j)$ is obtained using the Beta distribution loss curve, and $P(DS = ds_i \mid im_j)$ is obtained using the lognormal distribution fragility function.

Fig. 1 shows the risk curve calculated for a W1 (light frame wood) building. The intensity measure is peak ground acceleration (PGA). At each PGA, there is a probability distribution of losses, as shown using the 16th, 50th, and 84th percentiles in the left-bottom panel. We observe from the figure that the 50th percentile of losses in a W1 building with high-code design is similar to the 16th percentile losses in the same building with low-code design. This illustrates that a W1 building with low-code design is more likely to experience higher losses compared to one with high-code design for the same ground shaking. The probability distribution of loss at a given PGA is combined with the hazard information to compute the risk curve shown in the right panel of Fig. 1. Here, loss is given in terms of the loss ratio or the percent of total cost of a structure.

We observe from Fig. 1 that the 2016Induced hazard is two orders of magnitude higher than the 2014NatOnly hazard for Oklahoma City. Additionally, this hazard is greater than that in LA. This implies that in a short-term of a year, the hazard calculations predict a higher probability of exceedance for a given level of ground shaking in Oklahoma City than in LA. We observe that the risk in Oklahoma City from induced seismicity is also two orders of magnitude higher than its natural level. We also compare the risk curve for a W1 (light frame wood) structure in Oklahoma City and LA. We observe that although the hazard curves for 2014NatOnly LA and 2016Induced OKC are similar, the risk in Oklahoma City is an order of magnitude higher due to the difference in design code levels. Fig. 2 shows the risk curves calculated for each building type in our selected census block in Oklahoma City.

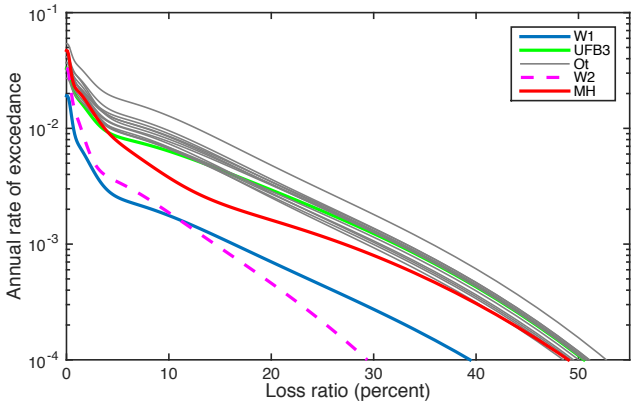

Figure 2 - Risk curves for different building types in Oklahoma City for the USGS 2016Induced hazard curve. The curves for building types that have been compressed into category *Others*, are shown here individually.

We have so far computed the risk curves for an individual building. To compute the cumulative losses for multiple buildings in a census block, we make the assumptions that the losses in individual buildings are independent of each other, and that the cost of each building of the same type equals the average cost for that building type.

We first compute the distribution of cumulative losses in the buildings of the same building type (like W1, W2, etc.). Due to the above stated assumptions, the losses in each building of the same building type are independent and identically distributed. Then the cumulative loss from buildings of the same type can be approximated using a normal distribution by applying the Central Limit Theorem (CLT) [12]. We use the building count shown in Table 1 to compute the mean and variance of the cumulative loss ratio. Using CLT, the cumulative mean loss ratio is equal to the mean loss ratio of a single building and corresponding standard deviation is equal to the standard deviation of a single building multiplied by the square root of the building count of that type. The normal distribution is additionally modified to a truncated normal distribution between 0 and the total cost of a building type. This is done since the loss cannot be less than zero, and we assume that it cannot exceed the total cost of a building. We verified by comparing with Monte Carlo simulations that the CLT approximation gives similar total losses; however, we have not included the verification approach in this paper.

We then combine the losses from each building type to compute the total loss in a census block. When combining different building types, we convert the loss ratios to dollar losses by multiplying the ratios with the building cost. The probability distribution of loss in a given building type given an intensity measure *im*, cannot be written as a standard continuous probability distribution, so we discretize it and compute the probability at $100 increment losses, as shown in Eq. (2).

$$\begin{aligned} Loss_{Tot} &= Loss_{W1} + Loss_{W2} + Loss_{UFB3} + Loss_{Ot} + Loss_{MH} \\ P(Loss_B = l \mid im_j) &= \sum_{i=1}^{n_{DS}} [P(Loss_B \geq l \mid ds_i, im_j) - \dots \\ &\qquad P(Loss_B \geq l + 100 \mid ds_i, im_j)] P(DS = ds_i \mid im_j) \end{aligned} \tag{2}$$

where $Loss_{Tot}$ refers to total loss in all buildings in the census block, and $Loss_B$ refers to loss in all buildings of type *B*.

The probability of total loss $P(Loss_{Tot})$, is obtained from the probability of losses from different building types by using the process of convolution, as shown in Eq. (3).

$$P(Loss_{Tot} = l \mid im_j) = (((Loss_{W1} * Loss_{W2}) * Loss_{UFB3}) * Loss_{MH}) * Loss_{Ot}(l) \tag{3}$$

where *A*B* refers to convolution of *A* and *B*, and is expressed as

$$A * B(x) = \sum_{a=0}^{x} P(A = a) \times P(B = x - a) \tag{4}$$

for some random variables *A* and *B* taking only non-negative values.

Finally to compute the probability of exceeding a given loss value $P(Loss_{Tot} > l \mid im_j)$, the probabilities at each loss value are added.

$$P(Loss_{Tot} > l \mid im_j) = 1 - \sum_{a=0}^{l} P(Loss_{Tot} = a \mid im_j) \tag{5}$$

Using the above formulation, we can now calculate the risk curve for all buildings in the census block by modifying Eq. (1) to Eq. (6) as shown below.

$$\lambda(Loss_{Tot} > l) = \sum_{j=1}^{n_{IM}} P(Loss_{Tot} > l \mid im_j) \lambda(IM = im_j) \tag{6}$$

This risk curve is shown in Fig. 3. The total cost of all buildings in the census block is $46.5 million. We observe from Fig. 3 that the cumulative risk from 2016Induced is almost two orders of magnitude higher than from 2014NatOnly. This implies that after including induced seismicity, the probability that a loss of $1 million in a

census block can be exceeded in a year is 1.33%, compared to 0.02% before the recent increase in seismicity. For a probability of exceedance of 1% in one year, we observe that the loss has increased from about $10,000 to $1.4 million after including induced seismicity.

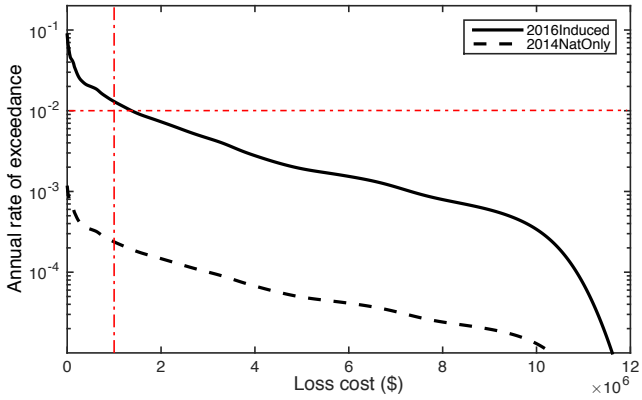

Figure 3 - Cumulative risk curve for a census block in Oklahoma City for USGS hazard curves, including and excluding induced seismicity.

3. Evaluation of Hazard and Risk

In this section, we describe the various parameters for which the sensitivity analyses are performed. These analyses are used to assess how changes in parameter values impact seismic hazard and risk. Hazard is calculated using Eq. (7) [13], and risk is calculated using Eq. (2-6), as described in the previous section. We continue with our site in Oklahoma City at coordinates 35.5° N and 97.5° W.

$$\lambda(IM > x) = \sum_{i=1}^{n_{sources}} \lambda(M_i > m_{min}) \sum_{j=1}^{n_M} \sum_{k=1}^{n_R} P(IM > x \mid m_j, r_k) P(M_i = m_j) P(R_i = r_k) \quad (7)$$

where λ(*E*) represents the rate of event *E*, *P*(*E*) is the probability of event *E*, $n_{sources}$ is the number of seismic sources, n_M is the number of discrete magnitude values considered, n_R is the number of discrete distance to site values considered, *IM* is an intensity measure, M_i is the magnitude for source *i*, and R_i is the source-to-site distance for source *i*.

USGS uses a logic tree approach to estimate hazard [1]. The first five levels of their tree correspond to magnitude distribution, and the last level to ground motion prediction equations. We describe these parameters, and the additional parameter - exposure, below.

3.1. Magnitude distribution

The USGS hazard maps utilize earthquake source models with Gutenberg-Richter (GR) earthquake magnitude distributions [1]. The distribution is characterized by *a*- and *b*-values, and is truncated with minimum and maximum considered magnitudes [13] (assuming that lower magnitude earthquakes will not affect buildings and larger magnitudes are not possible).

We assess the sensitivity of hazard and risk to both minimum and maximum magnitudes. We vary the minimum magnitudes from 2 to 5, and the maximum magnitudes from 5 to 8. USGS used a minimum magnitude of 2.7, and maximum magnitudes of 6 and 7.1 (with distribution) in their logic tree [1].

The *b*-values for induced earthquakes from wastewater injection have typically been found to be close to 1, similar to natural earthquakes. However, some authors have found the range to vary between 0.8 to 1.2 [14]. For induced seismicity from hydraulic fracturing, *b*-values as large as 2 have been observed [15]. We perform sensitivity analyses for *b*-values of 0.8, 1.0, and 1.2 for minimum magnitude 3, and maximum 8. Since only small magnitude earthquakes have been observed for hydraulic fracturing, we add *b*-values of 1.5 and 2 for minimum magnitude 2, and maximum 5.

The other parameter in the GR relation is the *a*-value. We change the rate of magnitude ≥ 3 (M≥3) earthquakes while keeping the *b*-value fixed, which has the effect of changing *a*-values. Based on change point analysis to determine seismicity rates in Oklahoma [16], we estimated a rate of about 75 earthquakes per year for M≥3 earthquakes within 0.5° latitude and longitude of our site. This is more than 100 times the rate used in 2014 USGS NSHM [9], and a similar order of increase as noted in the USGS 2016Induced report [1]. For sensitivity analysis, we consider M≥3 rates of 0.25, 2.5, 7.5, and 75 earthquakes per year (referred to as M3Rate_0.25, M3Rate_2.5, M3Rate_7.5, and M3Rate_75.0, respectively).

3.2. Ground motion prediction equation

Ground motion prediction equations (GMPE) are used to estimate the shaking from an earthquake at a site given certain parameters like earthquake magnitude, earthquake source-to-site distance, etc. There are a number of GMPEs available for the Central and Eastern US (CEUS). Atkinson and Boore (2006) (*ab06*) [18] is one of the GMPEs used for computing the CEUS hazard for the USGS NSHM [9]. We compare it with Atkinson (2015) (*atk15*), which is a GMPE developed for small magnitude induced earthquakes in CEUS [17]. These GMPEs and their parameters that we modify for comparison of hazard and risk are stated in Table 3.

Table 3 - GMPEs and their parameter values used for sensitivity analyses

Short name	Reference	Vs_{30} (m/s)	Stress (bars)
ab06	Atkinson and Boore (2006) [18]	400, 760	35, 140, 560
atk15	Atkinson (2015) [17]	760	

We analyze the impact of different parameters that are required for the GMPEs. One of these parameters is the average shear-velocity down to 30 m (Vs_{30}) at a site. The USGS topographic-slope-based estimate of Vs_{30} at our site is 400 m/s [19]. We analyze hazard and risk with another Vs_{30} value of 760 m/s for *ab06* since *atk15* GMPE is only developed for Vs_{30} of 760 m/s. The other parameter that we modify is the *stress* parameter in *ab06*. We use the default of 140 bars, but also compare with the extreme values of 35 bars and 560 bars.

3.3. Exposure

Exposure refers to the type of structural systems exposed to an earthquake. For the sensitivity analysis of exposure, we assess the change in risk from changing the code level of the structural design. We assess the change in risk for all buildings belonging to either low-code, moderate-code, or high-code design type.

4. Results of Sensitivity Analysis

We perform sensitivity analyses for the parameters described above. Each hazard and risk comparison also includes 2016Induced hazard and risk curves for Oklahoma City, described in section 2. These curves are provided only for reference, and are not intended to validate the correctness of any parameters used in the sensitivity analyses.

For all hazard and risk calculations, unless specified, the default value of minimum magnitude is 3, maximum magnitude is 8, *b*-value is 1, M≥3 rate is 75 earthquakes per year, GMPE is *atk15*, and exposure is low-code construction. Since the hazard and risk curves for regions of induced seismicity are intended for short-term like one year forecasts, we do not show PGA and losses corresponding to rates of exceedance less than 1×10^{-4}, which is almost equal to 0.01% probability of exceedance in 1 year.

4.1. Magnitude distribution

The hazard and risk curves for different minimum and maximum magnitudes are shown in Fig. 4. They are shown for different *b*-values and M≥3 rates in Fig. 5 and 6, respectively.

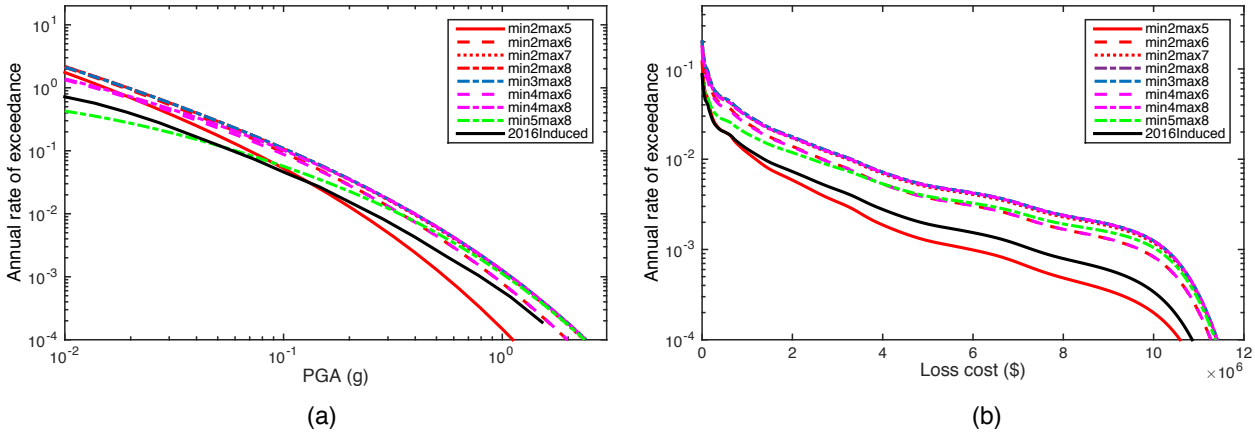

Figure 4 - Hazard (a) and risk curves (b) for different values of minimum and maximum magnitudes. Same minimum magnitudes have the same color, and same maximum magnitudes have the same linestyle.

We observe from Fig. 4 that the hazard corresponding to smaller PGA is governed by minimum magnitude, while that for larger PGA is governed by maximum magnitude. There is little difference in the hazard curves for minimum magnitude of 2 or 3. Since risk is influenced almost entirely by PGA values larger than 0.1g, as shown in Fig. 1, a minimum magnitude of less than 4 has little influence on risk. However, we observe that it is important to use a lower minimum magnitude than typically has been used for hazard assessments in Western North America, due to the lower seismic requirements for buildings in the CEUS.

We also observe from Fig. 4 that there is less increase in the rate of exceedance of a given PGA as the maximum magnitude increases. The hazard curve is an order of magnitude lower with a maximum magnitude of 5 compared to 8, but the increase becomes negligible for maximum magnitude of 7 versus 8. The increase in risk curve reduces similarly as the maximum magnitude increases. This implies that in Oklahoma, where an earthquake with magnitude 5.6 was observed in 2011, setting a maximum magnitude to 6 or above will have only a small influence on its hazard and risk. Note that we performed this analysis for a single census block, however larger magnitude earthquakes will affect larger areas and increase the total losses in an earthquake.

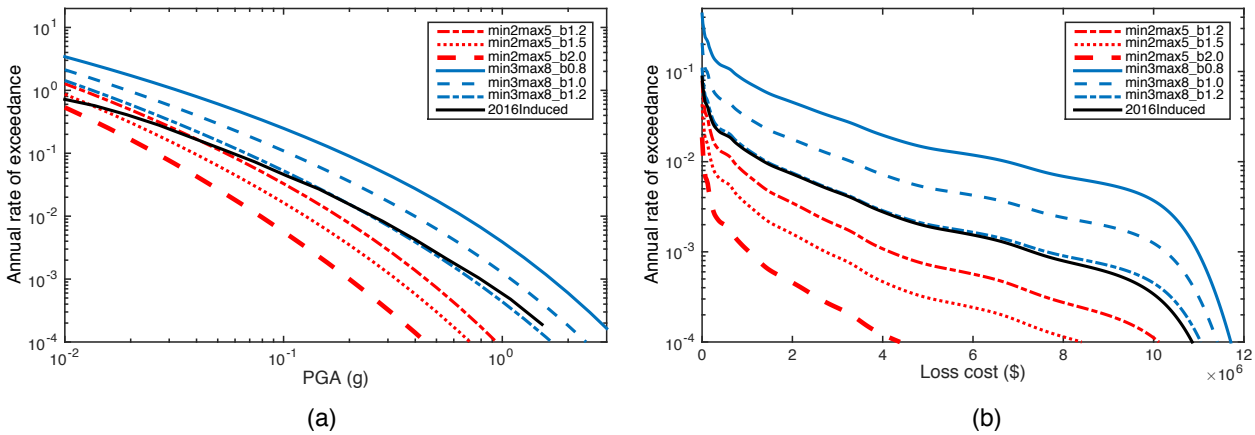

Figure 5 - Hazard (a) and risk curves (b) for different *b*-values at different minimum and maximum magnitudes. Same min-max magnitudes have the same color, and same *b*-values have the same linestyle.

We observe from Fig. 5 that hazard at a given PGA and risk at a given loss value reduce with increasing *b*-value. Since for these analyses, the rate of earthquakes is fixed at M≥3, a larger *b*-value implies fewer expected earthquakes of magnitudes larger than 3. This leads to a lower hazard at larger PGA for increasing *b*-value. The risk curve reduces by almost an order of magnitude by increasing the *b*-value from 0.8 to 1.2. From the figure, we

conclude that *b*-value is an influential parameter for hazard and risk assessment, and should be carefully constrained.

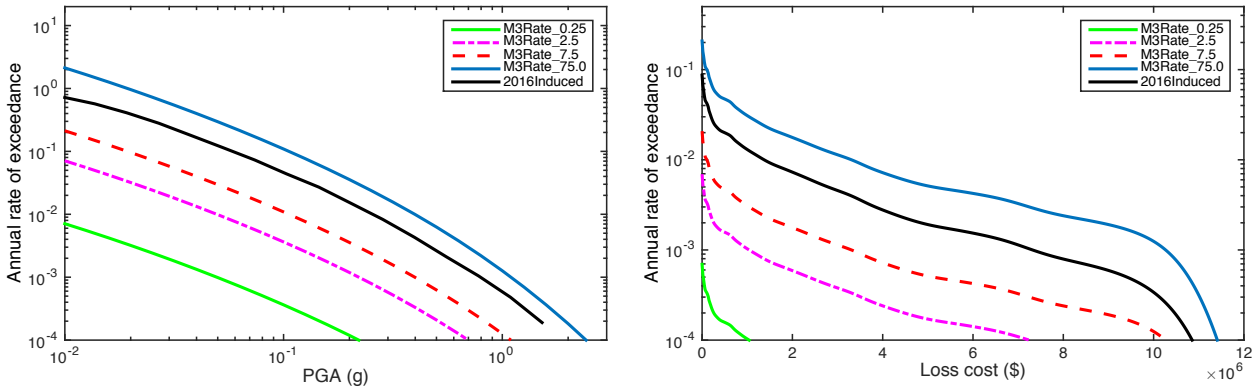

Figure 6 - Hazard (a) and risk curves (b) for different values of magnitude ≥ 3 annual earthquake rate.

The *a*-value also has a significant impact on both hazard and risk assessments. A 10-fold increase in earthquake rate, or a linear increase in *a*-value, increases the hazard and risk 10-fold. This has significant implications for regions like Oklahoma where recent short-term seismicity rate has been estimated to be more than 100 times the pre-2008 rate [1].

4.2. GMPE

The hazard and risk curves for different GMPEs and their parameters are shown in Fig. 7.

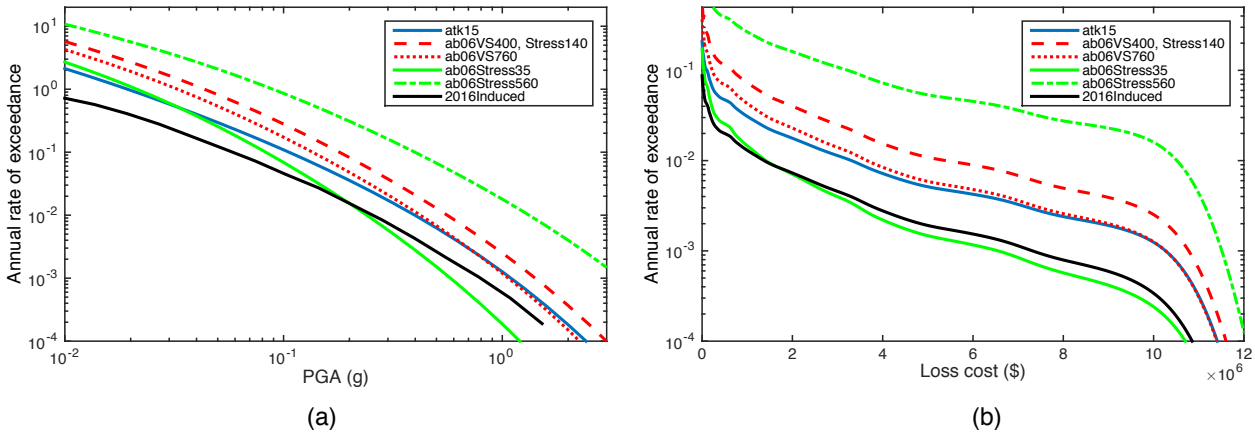

Figure 7 - Hazard (a) and risk curves (b) for different GMPEs and their parameters. Different Vs_{30} values are represented by different linestyles in red color, and different stress values are represented by different linestyles in green color.

We observe from Fig. 7 that the *atk15* and *ab06* at Vs_{30} = 760 m/s yield similar hazard and risk curves, especially at larger PGA and loss values. However, *ab06* with the estimated Vs_{30} = 400 m/s at our site yields higher hazard and risk curves. Increasing the *stress* parameter in *ab06* also increases both hazard and risk. This illustrates the impacts of site soil characteristics, and fault stress parameters on hazard and risk assessments.

4.3. Exposure

Exposure has no impact on hazard in our case since the rate of exceedance of a given PGA does not depend on the building inventory at the site. Hence, we use the 2016Induced hazard to evaluate changes in risk curves. The risk curves for buildings in different design levels (low-code, moderate-code, and high-code) are shown in Fig. 8.

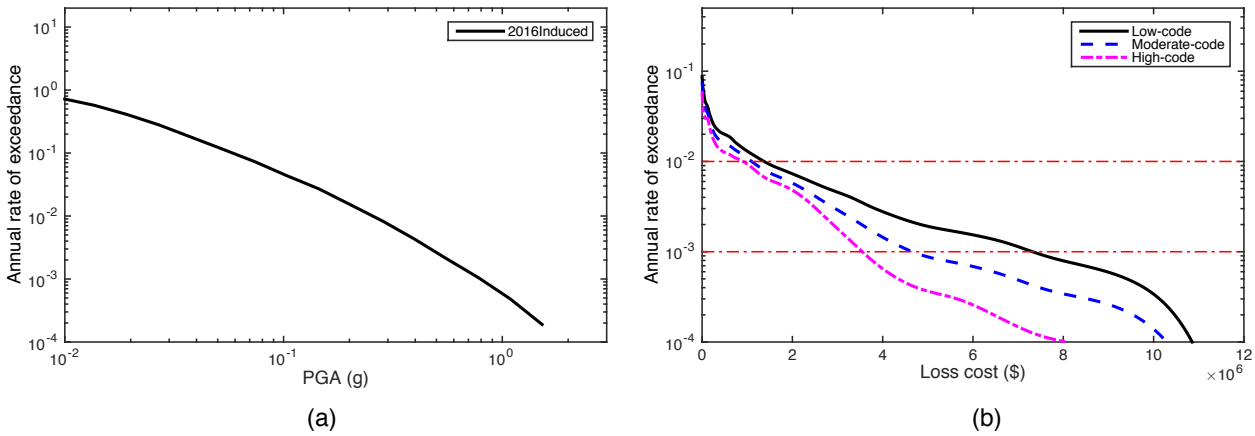

Figure 8 - (a) USGS 2016Induced hazard curve for Oklahoma City, and (b) risk curves for different code levels of buildings in a census block of Oklahoma City.

The risk curves from Fig. 8 match our expectation that buildings with higher seismic resistance have lower rates of exceedance of a given loss value. However, we observe that the risk is similar at lower loss values. This is because the low-value losses come primarily from unreinforced masonry buildings (UFB3) and mobile homes (MH) that have the same fragility functions at all code levels in HAZUS [2].

From the figure, the loss values corresponding to the probability of exceedance of 1% in one year are $1.4 million for low-code, $1.1 million for moderate-code, and $0.9 million for high-code. At a lower probability of exceedance of 0.1% in one year, the corresponding loss values are $7.3 million, $4.6 million, and $3.5 million. This implies that retrofitting is a potentially effective risk management strategy to counteract increased seismic activity, assuming that variation in performance among code levels used here is comparable to variation in performance of un-retrofitted and retrofitted buildings. This type of assessment can be used by stakeholders to perform cost-benefit analysis of retrofitting buildings in the vicinity of seismicity inducing operations.

5. Conclusions

In this paper, we studied how magnitude distribution, ground motion prediction equations, and building design standards affect the seismic hazard and repair cost risk. We also estimated this risk for a census block in Oklahoma City using the one-year induced seismicity hazard curve developed by USGS [1] and building data collected by HAZUS [2].

Due to increased hazard in Oklahoma City from including induced seismicity, the risk has increased significantly compared to the risk calculated using the hazard curve from USGS 2014 hazard maps [9]. We observed that for a 1% probability of exceedance in one year, the loss in a census block has increased from $10,000 to $1.4 million. In our assessment, the loss reduced from $1.4 million to $0.9 million if the buildings were assumed to satisfy higher seismic code provisions (e.g., as might be achieved via retrofitting). This type of assessment can be used to quantify the benefits of risk mitigation measures like retrofitting and can thus serve as a critical tool for developing a risk mitigation plan for regions of induced seismicity.

Our sensitivity analyses showed that the effect of the maximum considered earthquake magnitude on repair cost risk is small above a maximum magnitude of 6. The minimum magnitude must be lower than M5, that is typically used in Western North America, due to the historically lower seismic design provisions in the CEUS. We observed only small impacts on structural damage risk from lowering the minimum magnitude to less than 4. However, there could be impacts on non-structural components, and felt-shaking from lower magnitude

earthquakes. We note that the USGS 2016 induced seismicity hazard calculations consider a minimum magnitude of 2.7, which is very sufficient based on this analysis.

The *a*- and *b*-values in the Gutenberg-Richter relation significantly impact both hazard and risk. Increasing the earthquake rate at a given magnitude increases the hazard and risk by the same order. Keeping the earthquake rate fixed at the minimum magnitude and decreasing the *b*-value increases hazard and risk, due to a greater probability of observing larger magnitude events.

We observed from our sensitivity analysis for GMPE that for structural damage estimation, it is important to assess the ground motion attenuation in regions of induced seismicity for magnitudes larger than 4 earthquakes. The fault stress parameter, as described for *ab06*, and site soil characteristics were found to affect the hazard and risk. Developing GMPEs specifically for regions of induced seismicity is critical for developing better hazard and risk estimates.

Our risk estimate for a census block in Oklahoma City confirms that the seismic risk has increased substantially for the hazard curve that includes induced seismicity. Similar risk assessments at a community level can help in evaluating different risk mitigation approaches like retrofitting of buildings, relocating injection operations or population farther from each other, and protocols to lower seismic hazard [7, 20]. We developed the risk estimates only for structural damage, but the same approach can be used to include losses from non-structural components. Short term hazard and risk estimates can thus be used as decision support tools by regulators and stakeholders to understand and mitigate the impacts of seismicity inducing operations.

6. Acknowledgements

Funding for this work came from the Stanford Center for Induced and Triggered Seismicity.

7. References

[1] Petersen, M. D., Mueller, C. S., Moschetti, M. P., Hoover, S. M., Llenos, A. L., Ellsworth, W. L., Michael, A. J., Rubinstein, J. L., McGarr, A. F., and Rukstales, K. S. (2016). 2016 One-Year Seismic Hazard Forecast for the Central and Eastern United States from Induced and Natural Earthquakes. U.S. Geological Survey Open-File Report 2016-1035, Reston, VA.

[2] Holmes, W., Borcherdt, R., Brookshire, D., Eisner, R., Olson, R., O'Rourke, M., Lagorio, H., Reitherman, R., and Whitman, R. (2015). Hazus-MH 2.1 Technical Manual - Earthquake Model. Technical report, Department of Homeland Security, Federal Emergency Management Agency, Washington, DC.

[3] Ellsworth, W. L. (2013). Injection-Induced Earthquakes. *Science*, 341(6142):1225942.

[4] Keranen, K. M., Weingarten, M., Abers, G. A., Bekins, B. A., and Ge, S. (2014). Sharp increase in central Oklahoma seismicity since 2008 induced by massive wastewater injection. *Science*, 345(6195):448–451.

[5] Weingarten, M., Ge, S., Godt, J. W., Bekins, B. A., and Rubinstein, J. L. (2015). High-rate injection is associated with the increase in U.S. mid-continent seismicity. *Science*, 348(6241):1336–1340.

[6] Council, N. R. (2013). Induced Seismicity Potential in Energy Technologies. The National Academies Press, Washington, DC.

[7] Walters, R. J., Zoback, M. D., Baker, J. W., & Beroza, G. C. (2015). Characterizing and Responding to Seismic Risk Associated with Earthquakes Potentially Triggered by Fluid Disposal and Hydraulic Fracturing. *Seismological Research Letters*, *86*(4), 1110–1118.

[8] Mignan, A., Landtwing, D., Kstli, P., Mena, B., and Wiemer, S. (2015). Induced seismicity risk analysis of the 2006 Basel, Switzerland, Enhanced Geothermal System project: Influence of uncertainties on risk mitigation. *Geothermics*, 53:133–146.

[9] Petersen, M. D., Moschetti, M. P., Powers, P. M., Mueller, C. S., Haller, K. M., Frankel, A. D., Zeng, Y., Rezaeian, S., Harmsen, S. C., Boyd, O. S., Field, N., Chen, R., Rukstales, K. S., Luco, N., Wheeler, R. L., Williams, R. A., and Olsen, A. H. (2014). Documentation for the 2014 update of the United States national seismic hazard maps. Technical report, U.S. Geological Survey Open-File Report 20141091.

[10] Di Pasquale, G. and Goretti, A. (2001). Vulnerabilit funzionale ed economica degli edifici residenziali colpiti dai recenti eventi sismici italiani. In *proceedings of the tenth National conference LIngineria Sismica in Italia, Potenza-Matera, Italy*.

[11] Krawinkler, H. and Miranda, E. (2004). *Performance based earthquake engineering*, volume 9. CRC Press: Boca Raton, FL.

[12] Ross, S. M. (2009). *Probability and statistics for engineers and scientists*. Elsevier, Canada.

[13] Kramer, S. L. (1996). *Geotechnical earthquake engineering*. Pearson Education India.
[14] Benz, H. M., McMahon, N. D., Aster, R. C., McNamara, D. E., and Harris, D. B. (2015). Hundreds of Earthquakes per Day: The 2014 Guthrie, Oklahoma, Earthquake Sequence. *Seismological Research Letters*, 86(5):1318–1325.
[15] Friberg, P. A., BesanaOstman, G. M., and Dricker, I. (2014). Characterization of an Earthquake Sequence Triggered by Hydraulic Fracturing in Harrison County, Ohio. *Seismological Research Letters*.
[16] Gupta, A. and Baker, J. W. (2015). A Bayesian change point model to detect changes in event occurrence rates, with application to induced seismicity. In *12th International Conference on Applications of Statistics and Probability in Civil Engineering (ICASP12), Vancouver, Canada*.
[17] Atkinson, G. M. (2015). Ground Motion Prediction Equation for Small to Moderate Events at Short Hypocentral Distances, with Application to Induced Seismicity Hazards. *Bulletin of the Seismological Society of America*, 105(2a): 981-992.
[18] Atkinson, G. M. and Boore, D. M. (2006). Earthquake Ground-Motion Prediction Equations for Eastern North America. *Bulletin of the Seismological Society of America*, 96(6): 2181-2205.
[19] Wald, D. J. and Allen, T. I. (2007). Topographic Slope as a Proxy for Seismic Site Conditions and Amplification. *Bulletin of the Seismological Society of America*, 97(5):1379–1395.
[20] Bommer, J. J., Crowley, H., and Pinho, R. (2015). A risk-mitigation approach to the management of induced seismicity. *Journal of Seismology*, pages 1–24.